https://doi.org/10.1016/j.electacta.2019.04.007

Insights into the transition metal ion-mediated electrooxidation of glucose in alkaline electrolyte

*Weiran Zheng, Yong Li, Lawrence Yoon Suk Lee**

Department of Applied Biology and Chemical Technology and the State Key Laboratory of Chemical Biology and Drug Discovery, The Hong Kong Polytechnic University, Hung Hom, Kowloon, Hong Kong SAR, China.

*lawrence.ys.lee@polyu.edu.hk (L. Y. S. Lee)

Abstract

Glucose electrooxidation is of particular interest owing to its broad applications in glucose fuel cell and electrochemical sensing. In pursuit of high atomic utilization of catalytic active sites, we employed homogenously dispersed transition metal ions (Co^{2+}, Cu^{2+}, and Ni^{2+}) as the electrocatalyst in alkaline electrolyte. Combining cyclic voltammetry, chronoamperometry, impedance spectroscopy, and *in situ* UV-Vis spectroelectrochemistry, the catalytic activity and reaction mechanism of M(II)-catalyzed glucose electrooxidation are discussed, suggesting a general activity trend of Co(II) > Cu(II) > Ni(II). Using a μM level of Co(II), Cu(II), and Ni(II), the sensitivity values of 1,342, 579, and 38.9 mA M^{-1} cm^{-2} are achieved, respectively, toward glucose sensing. The coordination between metal sites and glucose plays the critical role of lowing the oxidation potential of M(II) to higher valent forms. A homogenous reaction mechanism is suggested: Co(II)-catalyzed reaction shows potential-dependent electrooxidation *via* the formation of Co(III)-glucose and Co(IV)-glucose complex, while both Cu(II) and Ni(II) feature the intermediate of M(III)-glucose. The Co(II)-glucose electrooxidation presents the smallest charge transfer resistance and the highest transfer coefficient, accounting for its high activity.

Keywords: glucose electrooxidation; cobalt; nickel; copper; *in situ* UV-Vis spectroelectrochemistry

1. Introduction

The electrooxidation of glucose is a critical reaction that lays the foundation for the development of non-enzymic glucose sensors and glucose fuel cells [1-3]. Currently, various metal and metal-based materials have been extensively used as the electrocatalyst, including Au [4], Pd [5], Pt [6], Co [7], Cu [8], Ni [9], showing reasonable catalytic activities. Given the low cost, the use of earth-abundant transition metals, such as Co, Cu, and Ni, are generally preferred, and their metallic, oxide and hydroxide forms have been widely employed. For Co species, $Co(OH)_2$ [10] and Co_3O_4 [11, 12] are the most common oxide forms engaged as the electrocatalysts. Likewise, many researchers utilized the diverse forms of Cu-based and Ni-based nanomaterials, such as CuO [13-15], Cu_2O [16], NiO [17], and $Ni(OH)_2$ [18, 19], for electrocatalysis.

Despite some ongoing debates over the mechanism of CuO-based material-catalyzed reactions [20], it is generally accepted that the redox properties of metal sites, involving their higher oxidation states, plays a crucial role in glucose electrooxidation [7-9]. Under the alkaline conditions, the electrooxidation of Co(II) to its Co(III) form (CoOOH) and Co(IV) form (CoO_2) [21, 22] are considered to be essential for glucose oxidation. Similarly, the production of Cu(III) form (CuOOH) [14] and Ni(III) (NiOOH) [23] plays the key role in glucose electrooxidation *via* Cu- and Ni-based catalysts. Therefore, in pursuit of high efficiency and stability, researchers have been adopting different methods to alter the structural and electronic properties of active sites. So far, most of the methods can be divided into two strategies. One common tactic is altering the electronic structure of metal through bimetallic structure formation, and different metals and combinations have been explored, such as CuCo[24] and CuNi [25]. In some reports, conductive composites, such as conductive polymers [8, 25, 26], graphene [27, 28], carbon nanotubes [29-31], are introduced as the catalyst support to improve the charge transfer between the metal sites

and the electrode. Another more straightforward strategy of improving the catalytic activity is to increase the numbers of active sites by enlarging the electrochemical surface area. Such a strategy leads to morphology-controlled deposition and synthesis of thin-layered or porous structures [7, 11, 32]. For example, Lu and co-workers [14] prepared uniform CuO nanowire array layers on a nanoporous Cu_2O film to maximize the numbers of Cu sites on the electrode. Based on the same idea, most recently, metal-organic frameworks (MOFs), including Co-MOFs [33], Cu-MOFs [34, 35], and NiCo-MOFs [36], have been used either directly as electrocatalyst or precursor for other nanocomposites. The even distribution of metal sites in the frameworks, in principle, can offer an atomic level exposure of metal sites. However, despite much-improved activities, the involvement of sophisticated nanostructures inevitably complicates the fabrication process and increases the cost. Moreover, the stability of many nanostructures under electrochemical conditions are yet to be improved.

Based on the same idea of maximizing the active sites, we have previously described a simple and efficient strategy towards glucose electrooxidation using Cu(II) species in an alkaline electrolyte [37, 38]. Different from the modified electrodes, the homogenously dispersed Cu(II) species, when engaged as the electrocatalyst, allow thorough interaction between metal sites and glucose. The complex of Cu(II)-glucose serves as the reactant near the electrode surface and gets oxidized to a Cu(III)-glucose intermediate, which eventually produces gluconate ion regenerating Cu(II) species [37]. The high efficiency of such Cu(II)-mediated catalytic system leads to the development of a series of electrochemical glucose sensors [8, 30]. Since Co and Ni share the similar redox properties and glucose electrooxidation mechanism [10, 39], their performance in such homogenous catalytic system is, therefore, of particular interest. So far, their catalytic properties towards glucose electrooxidation are not yet reported.

Herein, we investigate the electrochemical oxidation of glucose catalyzed by homogenously dispersed transition metal ions (Co^{2+}, Cu^{2+}, and Ni^{2+}) in the alkaline electrolyte. The electrochemical behaviors of metal ions and glucose are studied using cyclic voltammetry, and the kinetic aspects of different metal species towards glucose electrooxidation are evaluated. The reaction mechanisms of metal ion-mediated catalysis are proposed by the impedance spectra under various bias voltages in conjunction with the surface species information from *in situ* UV-visible (UV-Vis) spectroelectrochemical studies.

2. Experimental

2.1 Materials

Sodium hydroxide (>96%, Uni-chem), D-(+)-glucose (>99.5%, Sigma-Aldrich), copper(II) nitrate hydrate (99.999%, Sigma-Aldrich), cobalt(II) nitrate hexahydrate (99.999%, Sigma-Aldrich), and nickel(II) nitrate hexahydrate (99.999%, Sigma-Aldrich) were used as received. All aqueous solution was prepared using double-deionized water (DI water, R > 18.2 MΩ cm^{-1}) produced by MilliQ Water System (Millipore, USA).

2.2 Electrochemical characterization

Glassy carbon electrode (GCE, 3 mm diameter, surface area = 0.071 cm^2) was polished with 1.0, 0.3, and 0.05 μm α-Al_2O_3 powders (CH Instruments) and then rinsed with DI water and acetone repeatedly. The cleaned GCE electrode was dried at room temperature before used as a working electrode.

For all electrochemical characterization, a three-electrode system was used with saturated calomel electrode (SCE, 25 °C) and Pt wire as the reference and counter electrode, respectively. The electrolyte was 0.1 M NaOH aqueous solution degassed with N_2 for 30 mins before the electrochemical test. Cyclic voltammetry (CV) and electrochemical impedance spectroscopic (EIS)

measurements were conducted on a PARSTAT MC (PMC1000/DC) electrochemical system (Princeton Applied Research, USA). The scan rate of CV was 5 mV s^{-1} for all measurements. The EIS results were collected from 1 MHz to 10 mHz at various applied potentials with an amplitude of 10 mV RMS. The amperometric *i*-t electrochemical measurements were performed on a CHI 1030A electrochemical analyzer (CH Instruments, Inc., USA) with continuing magnetic stirring at 1,070 rpm.

For *in situ* UV-Vis spectroelectrochemical studies (SPECE), an integrated spectroelectrochemical system (including an AvaLight UV/Vis/NIR light source, an AvaSpex-UL S2048 Fiber-Optic spectrometer, and a WaveDriver 20 benchtop potentiostat/galvanostat System, Pine Research Instrumentation, Inc., USA) was used. The spectroelectrochemical cell uses a gold honeycomb electrode as both the working and counter electrode and SCE is used as the reference electrode. A staircase cyclic voltammetric (SCV) method was used for the UV-Vis spectroelectrochemical study with an amplitude of 5 mV and a period of 20 s.

3. Results and Discussion

3.1 Potential sweep study

Before the electrochemical studies, the metal ions (0.5 μM ~ 1.0 mM) were added to 0.1 M NaOH (pH=12.96) aqueous solution to reach equilibrium. According to the Pourbaix diagrams of Co, Cu, and Ni (**Figure S1**), the soluble metal species are formed *via* the following reactions:

Co:

$$Co^{2+}+3OH^- \rightarrow Co(OH)_3^- \quad (1a)$$

and/or $$Co^{2+}+3OH^- \rightarrow HCoO_2^-+H_2O \quad (1b)$$

Cu:

$$Cu^{2+}+4OH^- \rightarrow Cu(OH)_4^{2-} \quad (2a)$$

and/or $Cu^{2+}+3OH^- \rightarrow HCuO_2^- + H_2O$ (2b)

Ni:

$Ni^{2+}+3OH^- \rightarrow Ni(OH)_3^-$ (3a)

and/or $Ni^{2+}+3OH^- \rightarrow HNiO_2^- + H_2O$ (3b)

Under the experimental conditions of room temperature and M(II) species (M = Co, Cu, and Ni) concentration between 0.5 μM and 1.0 mM, the formation of soluble $M(OH)_n^{2-n}$ (n = 3, 4) and HMO_2^- are expected.

(Figure 1)

The electrochemical behaviors of the soluble metal species in an alkaline electrolyte with and without different concentration of glucose (1, 5, and 10 mM) were studied by the CV method using bare GCE, and the plots are shown in **Figures 1a-1c.**

In 0.1 M NaOH electrolyte, only non-Faradaic current signals due to the formation of the electrochemical double layer on GCE can be observed within the applied potential range of 0 ~ 1.0 V. Upon the addition of 1 mM of M(II), the current density increases in all three voltammograms. Such enhancements are attributed to the electrooxidation of M(II) species to their higher oxidation states and the accomplished oxygen evolution reaction (OER) after the potential exceeding the reaction threshold ($E°$ = 223 mV *vs*. SCE, pH=12.96) [40-42]. Specifically, for Co, starting from around 610 mV (inset of **Figure 1a**), the electrooxidation of Co(II) species ($Co(OH)_3^-$ and $HCoO_2^-$) to Co(III) (CoOOH) and Co(IV) species occurs (**Equations 4a, 4b,** and **4c**). As the potential precedes the discharge of oxygen, the Co(III) to Co(IV) (mainly CoO_2) electrooxidation predominates [40], resulting in a high current density of 23.1 mA cm^{-2} at 1.0 V. Such Co(IV) species only exist as an intermediate for OER (**Equation 4d**) [43, 44]. However, as shown in **Figure 1a**, the Co(II)/Co(III) and Co(III)/Co(IV) processes are hard to distinguish as the anodic

current shows no peaks. For Cu, the Faradaic current evolving from 660 mV (**Figure 1b**) is due to the oxidation of Cu(II) ($Cu(OH)_3^-$ and $HCuO_2^-$) to Cu(III) (CuO_2^-, CuOOH, and/or $Cu(OH)_4^-$, **Equation 5a**) [41]. As to Ni, the electrooxidation of Ni(II) species starts at around 520 mV (**Figure 1c**) and produces NiOOH as the primary form of Ni(III) species [42]. As potential further increases, the coupled OER occurs, and the water oxidation current would predominate (**Equation 5b**) [45, 46].

M = Co:

$$Co(OH)_3^- \rightarrow CoOOH + H_2O + e^- \quad (4a)$$

$$Co(OH)_3^- + OH^- \rightarrow CoO_2 + 2H_2O + 2e^- \quad (4b)$$

$$CoOOH + OH^- \rightarrow CoO_2 + H_2O + e^- \quad (4c)$$

$$CoO_2 + OH^- \rightarrow CoOOH + O_2 \quad (4d)$$

M = Cu, Ni:

$$M(OH)_3^- \rightarrow MOOH + H_2O + e^- \quad (5a)$$

$$MOOH + 4OH^- \rightarrow M(OH)_3^- + O_2 + H_2O \quad (5b)$$

As shown in **Figures 1a-1c**, the injection of glucose to the alkaline electrolyte containing 1 mM soluble M(II) species caused dramatic change to the CV plots. For Co(II), a current boost is evident from 420 ~ 610 mV compared with the Co(II) electrooxidation current obtained without glucose (inset of **Figure 1a**), indicating glucose electrooxidation. In this potential range, the measured current was directly related to the glucose concentration. At the potentials higher than 610 mV, the current is significantly lower than the Co(II) electrooxidation current. In the presence of glucose, a peak is observed, of which position depends on the glucose concentration: 826 mV (1 mM glucose), 853 mV (5 mM glucose), and 878 mV (10 mM glucose). Interestingly, from 610 to 930 mV, the higher glucose concentration is, the lower current is observed, until the potential

exceeds 930 mV where higher glucose concentration, again, gives a higher current signal. For Cu(II) and Ni(II), as shown in **Figures 1b** and **1c** respectively, the current increases after glucose addition within the studied potential range, and higher glucose concentration causes a higher current signal. The onset potential for glucose electrooxidation is found to be 330 mV using 1 mM Cu(II) and 470 mV using 1 mM Ni(II). In the first forward scans of glucose electrooxidation using Cu(II) and Ni(II), no distinct peak is shown, suggesting that the mass transfer limitation is not reached under the studied conditions in Cu(II)- and Ni(II)-catalyzed system. The possible effect caused by Cl^- ion from the SCE is addressed in the SI, where the CV results are confirmed to be valid by replacing SCE with Hg/HgO (1.0 M KOH) reference electrode, as shown in **Figure S2**.

For Co(II), Cu(II), and Ni(II), the onset potentials for glucose electrooxidation *via* M(II) are generally lower than that of M(II) electrooxidation (Co(II): 420 mV compared with 610 mV; Cu(II): 330 mV compared with 660 mV; and Ni(II): 470 mV compared with 520 mV). Considering that M(II) electrooxidation to its higher oxidation states is essential for both glucose electrooxidation and OER, it is reasonable that the intermediate (glucose-coordinated M(II), or M(II)-glucose complex) is oxidized easier than M(II) surrounded by only OH^- (M(II)-OH). In the case of Co(II), Co(II)-glucose electrooxidation occurs between 420 and 610 mV, while the Co(II)-OH electrooxidation have not started yet (or at a very low rate). The increasing glucose concentration causes electrooxidation current to increase. However, at potential higher than 610 mV, the Co(II)-OH electrooxidation current exceeds the glucose electrooxidation, an indicative of a kinetically faster OER comparing with the glucose electrooxidation. The current is a combined result of both OER (mediated by Co(II)-OH) and glucose electrooxidation (mediated by Co(II)-glucose). The addition of glucose reduces the total concentration of Co(II)-OH by forming Co(II)-glucose, resulting in the decrease of total current. Moreover, a higher glucose concentration decreases the

current. In other words, the addition of glucose to Co(II) solution prevents the OER *via* Co(II). For Cu(II) and Ni(II), the anodic current is higher in the presence of glucose, implying that glucose electrooxidation is faster than the electrooxidation of Cu(II)-OH and Ni(II)-OH.

To understand the kinetic aspects of glucose electrooxidation, we constructed the Tafel plots within the glucose electrooxidation range as **Figure 1d** (kinetic parameters obtained from different techniques are summarized in **Table 1**). For Co(II), two kinetic regions are found: one with a Tafel slope of 362 mV dec^{-1} between 520 and 650 mV, and the other with a Tafel slope of 117 mV dec^{-1} between 650 and 820 mV. The former can be attributed to the electrooxidation of Co(II)-glucose to Co(III)-glucose (charge transfer coefficient $\alpha = 0.157$), whereas the latter is correlated to the further oxidation of Co(III)-glucose to Co(IV)-glucose at a faster reaction rate ($\alpha = 0.503$). Cu(II)-catalyzed reaction also shows two distinct linear regions: 500 ~ 640 mV (549 mV dec^{-1}, $\alpha = 0.107$) and 640 ~ 900 mV (271 mV dec^{-1}, $\alpha = 0.219$), revealing a multistep electrochemical process of glucose oxidation depending on the applied potential. The first region shows a relatively slow process compared to the second one. It is commonly known that Cu(II) can react with glucose through a redox reaction of Cu(II)-glucose complex to produce Cu(I) species, which is utilized as Benedict's reagent. At room temperature, we indeed observed a color change in the electrolyte containing both Cu(II) and glucose, from sky blue to brown blue within one day at room temperature. Due to the short time required for CV (typically 400 s), the concentration of produced Cu(I) species is minor compared to Cu(II) (see Figure S3, SI for detailed discussion). Thus, the first kinetic region indicates the electrooxidation of produced Cu(I) species to Cu(II) species. This process is rather slow due to the rate limiting Cu(I) production *via* redox chemistry. The second region shows the dominating faster Cu(II)-glucose to Cu(III)-glucose electrooxidation. In the case of Ni(II), the relation of log *j* and applied potential remains linear within 600 ~ 900 mV, indicating

a single-step glucose electrooxidation (285 mV dec^{-1}, $\alpha = 0.209$) catalyzed by Ni(II). Therefore, at an applied potential higher than 600 mV, the Co system possesses the highest reaction rate, followed by Cu, and Ni, as suggested by both Tafel slopes and charge transfer coefficients.

(Table 1)

The stability of the M(II)-catalyzed glucose electrooxidation was studied using 1 mM M(II) and 5 mM glucose. **Figure 1e** shows the current-time (*i*-t) plots of Co(II), Cu(II), and Ni(II) at 600 mV. A current boost is observed in all systems after adding glucose. After the initial 2,000 s, the highest current density of 97.8 μA cm^{-2} is achieved using Co(II) catalyst, followed by 61.2 μA cm^{-2} using Cu(II), and 24.1 μA cm^{-2} using Ni(II). After 8,000 s, the current density changes to 99.3, 55.3 and 31.9 μA cm^{-2}, respectively, showing a current increment by 1.53 % and 32.4 % for Co(II) and Ni(II), while a decrement by 9.64 % for Cu(II). Nevertheless, such mild changes over long time indicate the high stability of all three catalysts in the alkaline electrolyte.

3.2 Catalytic performance evaluation

(Figure 2)

The electrochemical catalytic performance of metal ions towards glucose electrooxidation is evaluated by chronoamperometry following the procedure described in **Figure 2a**. Under continuous stirring, a target potential was applied to GCE until the background current stabilized. Then, a pre-determined amount of M(II) was introduced to the electrolyte at 100 s causing a current increment of Δi. Such current is due to the electrooxidation of M(II) to its higher valent form, or OER if the water electrooxidation potential is reached. Upon the stabilization of current signal, glucose was added to the electrolyte at 600 s, resulting in the further current boosts of $\Delta i'$ and $\Delta i''$ which are dependent on the glucose concentration. Sensitivity value, the current density increment caused by a certain amount of glucose under given conditions (M(II) concentration and applied

potential), is used to evaluate the catalytic activity.

We first determined the optimal reaction potential for glucose electrooxidation using M(II). **Figure 2c** (Co) and **Figure S4** (Cu and Ni) show the amperometric response of GCE to two concentrations of glucose (100 μM and 1.0 mM, respectively) in 0.1 M NaOH electrolyte containing 0.1 mM M(II) under various applied potentials (400, 450, 500, 550, 600, and 650 mV). At the applied potentials >550 mV, the significant current increment of Δi indicates the Co(III) to Co(IV) electrooxidation coupled with the discharge of oxygen, noted as OER current. Upon the addition of glucose, a further current boost evolves which quickly decays and stabilizes. In particular, at 650 mV, the current decreases rapidly causing the total current increment Δi_{total} drops below the OER current. The reasonable explanation is that glucose molecules occupy the coordination sites of Co(II) preventing the essential Co(II)-OH^- coordination for OER.

(Figure 3)

Since most of the reported catalysts are used as glucose sensors, we used the sensitivity value (current response to a certain amount of glucose: $\Delta i/\Delta c$), which is commonly reported, to evaluate the catalytic activity of the M(II)-catalyzed system and compare with other catalysts. High sensitivity indicates high activity towards glucose electrooxidation. **Figures 3a-3c** summarizes the sensitivity values obtained from three amperometric tests using 0.1 mM M(II) as the catalyst under various potentials. An optimal potential (Co: 600 mV; Cu: 600 mV; Ni: 500 mV) is found to achieve the highest sensitivity towards glucose. Below the optimal potential (and above onset potential), the reaction rate is expected to increase with the increasing potential according to the Tafel equation. While at a higher potential, both OER and glucose electrooxidation are competing for limited M(II) sites, limiting the reaction rate of glucose electrooxidation. As shown in **Figures 2c** and **S4b**, the current increment upon Co and Ni ion introduction (Δi) at 600 and 650 mV,

respectively, is much higher than that at lower potentials. Such high current enhancement reveals the substantial contribution of OER. At the optimal potential, the highest sensitivity is calculated to be 1,187 mA M^{-1} cm^{-2} using 0.1 mM Co(II), much higher than when Cu(II) (562 mA M^{-1} cm^{-2}) and Ni(II) (25.0 mA M^{-1} cm^{-2}) were used with the same concentration, confirming the general catalytic activity trend of metal ion towards glucose electrooxidation, Co(II) > Cu(II) > Ni(II). Under the conditions of an applied potential of 550 mV and M(II) concentration of 0.1 mM, the reaction rate of Co(II)-catalyzed glucose electrooxidation is ~2.8 and ~50 times higher than those catalyzed by Cu(II) and Ni(II), respectively. Despite the high sensitivity value, the inhibition of competing OER is highly desired for precious estimation of glucose electrooxidation *via* M(II). Thus, the optimal potential for glucose electrooxidation of 550 mV (Co), 600 mV (Cu), and 550 mV (Ni) is chosen to rule out the influence of OER current.

The correlation between M(II) concentration and glucose electrooxidation rate was studied at the chosen potentials. The amperometric responses are shown in **Figure S5**, and the corresponding sensitivity is plotted against M(II) concentration in **Figures 3d-3f**. The trend of sensitivity follows a volcano shape as the highest sensitivity is obtained at the medium M(II) concentration. At low M(II) concentrations, adding additional M(II) would enhance the sensitivity by providing more active sites for glucose coordination and electrooxidation. However, too much M(II) can result in a higher kinetic barrier for mass transfer to the GCE surface. **Figure 3d** shows that, for Co, the highest sensitivity of 1,342 mA M^{-1} cm^{-2} is achieved by using 5 μM Co(II) in 0.1 M NaOH aqueous solution. For Cu and Ni, the highest values of 579 and 38.9 mA M^{-1} cm^{-2} are demonstrated by using 200 μM Cu(II) and 10 μM Ni(II), respectively. Generally, given the same M(II) concentration, Co(II) shows the highest catalytic activity, followed by Cu(II) and Ni(II).

The catalytic activities of our Co(II)-, Cu(II)-, and Ni(II)-catalyzed glucose electrooxidation

were compared with other electrocatalysts recently reported as shown in **Table 2**. As stated before, most of the electrocatalysts were reported as glucose sensors, thus, it would be most suitable to compare the sensitivity values for catalytic activity evaluation. Clearly, the transition metal ion-mediated glucose electrooxidation system shows comparable, if not better, results to most of recently reported electrocatalysts.

(Table 2)

Table 2. Comparison of the Co(II), Cu(II), and Ni(II)-ion catalyst with other state-of-the-art electrocatalysts (in 0.1 M alkaline electrolyte, if not stated otherwise).

Electrocatalyst	Applied potential	Sensitivity ($\mu A\ mM^{-1}\ cm^{-2}$)	Year	Reference
Au@Cu_2O	0.6 V vs. SCE	715	2017	[47]
Pd nanocubes	−0.05 V vs. Ag/AgCl/3 M KCl	74	2016	[5]
Co/rGO/PPy	0.4 V vs. SCE	297.7	2017	[7]
Co_3O_4@nanoporous carbon	0.56 V vs. Ag/AgCl	249.1	2018	[12]
$Co(OH)_2$/rGO	0.5 V vs. Ag/AgCl	1246 (0.05 M NaOH)	2018	[10]
$Co(OH)_2$ NPs/3DGFs	0.45 V vs. SCE	2410	2019	[48]
Cu-C_3N_4/MWCNT	0.6 V vs. SCE	929	2018	[30]
CuO nanorods	0.55 V vs. Ag/AgCl	1319	2019	[49]
Cu-MOF	0.5 V vs. SCE	89	2018	[50]
NiO	0.55 V vs. Ag/AgCl	206.9 (0.5 M NaOH)	2019	[51]
$Ni(OH)_2$/rGO/Cu_2O	0.65 V vs. SCE	5350	2018	[52]
$Ni(OH)_2$	0.52 V vs. SCE	12.09	2018	[53]
NiO	0.52 V vs. SCE	24.0	2018	[54]
Co(II) 5 µM	0.55 V vs. SCE	1342		This work
Cu(II) 200 µM	0.60 V vs. SCE	579		This work
Ni(II) 10 µM	0.55 V vs. SCE	38.9		This work

rGO: reduced graphene oxide; PPy: polypyrrole; PANI: polyaniline; NPs: nanoparticles; 3DGFs: three-dimensional graphene frameworks.

3.3 Electrochemical impedance spectroscopy study

Electrochemical impedance spectroscopy (EIS) was employed to investigate the mechanism of glucose electrooxidation *via* M(II). The frequency response of GCE was studied in 0.1 M NaOH solution containing 1 mM M(II) and 1 mM M(II) + 5 mM glucose within the frequency range between 1 MHz and 10 mHz at a bias potential of 650 mV where the glucose electrooxidation took place. **Figures 4a-4c** shows the measured Nyquist plots of M(II) electrocatalytic systems in 0.1 M NaOH solution, together with the plot of GCE for comparison.

(Figure 4)

In the presence of 1 mM Co(II) (**Figure 4a**), the high frequency (HF) range shows a depressed semicircular arc, and the low frequency (LF) range features a horizontal line. The arc shape is typical for a single-step charge transfer reaction kinetically controlled in the HF time domain, which can be assigned to Co(III) to Co(IV) electrooxidation process (charge transfer resistance R_{ct} =1.93 kΩ). The linear region is associated with the diffusion-controlled electrooxidation. However, the phase angle is ~0°, suggesting an ignorable diffusion resistance [54]. The main reason is that the locally formed Co(IV) (**Equations 4b** and **4c**) can reproduce Co(III) species within the double layer region of GCE through OER (**Equation 4d**) to avoid mass transfer process of Co(II) from the bulk electrolyte. Upon the addition of glucose, HF indicates a larger depressed semicircular arc and a straight line at LF. The former is due to the glucose electrooxidation catalyzed by Co(II), showing the R_{ct} of 8.98 kΩ, while the following flat line indicates the bounded diffusion. The considerably larger R_{ct} in the presence of glucose suggests that the OER has been inhibited by a kinetically slower glucose electrooxidation, which is in good agreements with the CV results. Since the concentration of glucose is 5 times higher than that of Co(II) species, glucose molecules can occupy the coordination sites of Co(II). Similar to OER, the flat tail shows a confined mass transfer within the double layer region, presumably due to the local generation of Co(III) species.

The EIS profile of Cu(II) electrocatalyst differs from that of Co. At a bias voltage of 650 mV without glucose, only a large arc is evident (only a enlarge part is shown in **Figure 4b** for clarity) in the studied frequency range, with an R_{ct} of 95.5 kΩ. The absence of diffusion-controlled region implies that the Cu(II) to Cu(III) electrooxidation, despite high charge transfer resistance (large energy barrier), is kinetically controlled by charge transfer even at LF range (down to 10 mHz). Notably, the EIS profile shows two distinct depressed semicircular arcs when Cu(II) and glucose

co-exist in the electrolyte, indicating the existence of two time constants. The one in the HF region is due to the charge transfer process from intermediate to the electrode, and the other in the LF region is due to the adsorption of the intermediates on the GCE surface. Moreover, the adsorption (16.7 kΩ) and charge transfer resistance (18.4 kΩ) in the Cu(II)-catalyzed system is much higher than that in the Co(II)-catalyzed system.

Figure 4c shows the Nyquist plots of GCE in the electrolyte containing 1 mM Ni(II) as the catalyst. A large semicircle associated with the electrooxidation of Ni(II) to Ni(III) is shown with an R_{ct} of 81.1 kΩ. After adding glucose, two overlapping depressed semicircles evolve showing a reduced R_{ct} of 37.4 kΩ. Similar to that of Cu(II), the larger one at the HF region is due to the electron transfer process of glucose electrooxidation, while the smaller one at the LF region can be attributed to the adsorption process of the intermediates. Notably, at a bias voltage of 650 mV, the charge transfer resistance of metal electrooxidation is larger than that of glucose electrooxidation *via* metal ion for Cu(II) and Ni(II), while Co shows the opposite.

To resolve the reaction route, we studied the frequency response of glucose electrooxidation *via* Co at various bias potentials (500, 550, 600, and 650 mV), and the Nyquist plots are shown in **Figure 4e**. The corresponding Nyquist plots for Cu(II) and Ni(II) are shown in **Figure S6.** As indicated by CV results (**Figure 1a**), the electrooxidation of Co(II) starts at around 610 mV, whereas that of glucose barely starts from 450 mV. Therefore, the large semicircles produced in the electrolyte with only Co(II) under a bias voltage of 500 and 550 mV are due to the adsorption of Co(II) species on GCE. After introducing glucose, these semicircles exhibit smaller diameters, suggesting that glucose electrooxidation *via* Co(II) is favorable at 500 and 550 mV. Similar results were observed from the Ni(II) and Cu(II) cases. However, under a bias potential of 600 mV and higher, however, the semicircles due to the electrooxidation of Co(II) (**Equations 4a, 4b, 4c,** and

4d) present a smaller diameter than those of corresponding glucose electrooxidations, indicating that the glucose electrooxidation is kinetically slower than the OER-coupled Co(III)/Co(IV) oxidation. Conversely, glucose electrooxidation is always faster than the M(II) electrooxidation under the studied potential range when Cu(II) and Ni(II) are used.

To simplify our discussion, the electrooxidation process can be uniformly described by the equivalent electrical circuit shown in **Figure 4d**, in which R_s indicates the non-compensated resistance and R_{ct} represents the charge transfer resistance [54]. The double layer capacitance is demonstrated by a constant phase element (CPE) C_{dl} as implied by the depressed shape of experimental data. Although the diffusion-controlled process is not evident at the lowest frequency (10 mHz) studied in some Nyquist plots, the finite-length Warburg impedance with resistance cutoff is shown in Cu(II) and Ni(II) systems. Therefore, a Warburg diffusion element (Z_w) is added to mimic the mass transfer resistance of finite diffusion in the supported electrolyte [48]. After fitting the complex plane using the proposed equivalent circuit, the values of R_s and R_{ct} are obtained (**Table S1**) and plotted in **Figure 5**.

(Figure 5)

The non-compensated resistance (R_s), including the resistance of the electrolyte, the circuit, and the electrodes, which should be independent of the applied potential. As shown in **Figure 5**, the R_s values obtained from M(II) and M(II)+glucose systems at different bias voltages between 450 and 650 mV show only negligible decrement. Specifically, the R_s changes from 86.2 to 85.7 **Ω** for Co(II), and from 92.4 to 90.7 **Ω** for Co(II) + glucose. In the case of Cu(II), the R_s decreases slightly from 78.2 to 77.8 **Ω**, and from 87.4 to 87.1 **Ω** after adding glucose. As to Ni(II), the R_s drops from 84.7 to 84.1 **Ω**, and from 87.3 to 85.9 **Ω** with glucose introduced. The stable R_s values under different reaction conditions show that no coating layers (that could cause extra resistance)

are formed on the surface of GCE either during the M(II) electrooxidation or the glucose electrooxidation. Nevertheless, the R_s value varies with different M(II) used. Despite the same 0.1 M NaOH aqueous solution used as the electrolyte, this difference in R_s arises from the different equilibrium constant of M(II) species in the electrolyte. Notably, after adding glucose to the M(II) alkaline solution, the solution resistance increases by 5.0 Ω (Co), 9.3 Ω (Cu), and 1.8 Ω (Ni), which can be attributed to the lowered total ion strength in electrolyte due to the formation of M(II)-glucose complex.

The charge transfer resistance (R_{ct}) of M(II) electrooxidation and M(II)-catalyzed glucose electrooxidation, on the other hand, show a clear descendent trend with potential. Such a trend is expected as $R_{ct} = \frac{RT}{nFi_0}$, where R is the universal gas constant, T is temperature, n is the electron transfer number, F is the Faraday constant, and i_o is the exchange current density [56]. In the presence of M(II) only, the electrooxidation of M(II) to its higher valent form is kinetically hindered until the oxidation potential is reached, accompanied by dramatic decrease of R_{ct} to 11.36 kΩ (Co at 600 mV), 95.5 kΩ (Cu at 650 mV), and 148 kΩ (Ni at 600 mV). After adding glucose, the R_{ct} values are reduced, showing the faster rates of glucose electrooxidation than M(II)-OH electrooxidation, except for Co(II) at 600 and 650 mV. As stated previously, the glucose inhibits the essential Co(II)-OH^- coordination to suppress the kinetically favored OER.

3.4 In situ UV-Vis spectroelectrochemical studies

(Figure 6)

In situ SPECE is a powerful tool for analyzing the reaction mechanism, especially of homogenous electrocatalysis [37]. Herein, we studied the electrochemical behavior of Co(II), Cu(II), and Ni(II) in a 0.1 M NaOH solution with and without glucose as a function of applied potential **(Figure 6)**. Different from previous studies, the concentration values of both metal ions

and glucose are reduced to 0.2 and 0.5 mM, respectively, to ensure good signal-to-noise ratio while not reaching the saturation of the detector. The experimental setup of the in situ SPECE is shown in the supporting information as **Figure S7a**, and the possible interference due to the Au honeycomb electrode has been ruled out as shown in **Figure S7b**.

For Co, no significant change is observed until the potential reaches 850 mV at which three distinguishable signals appear at 365, 511, and 632 nm. They are due to the formation of Co_3O_4 (a combination of Co(II) and Co(III) species) [57]. The negative peak at 230 nm indicates the consumption of $Co(OH)_3^-$ species. The spectra obtained in the presence of glucose, however, shows a different trend with a broad peak(s) between 250 and 500 nm forms at 950 mV, suggesting the formation of $Co(OH)_2$ [58, 59]. Such difference shows that Co_3O_4 formation during OER is impeded by glucose, possibly forming Co(III)-glucose and Co(IV)-glucose species. Meanwhile, the $Co(OH)_3^-$ consumption peak vanishes, indicating a different species such as Co(II)-glucose complex. As per Cu(II), two distinctive peaks at 273 and 362 nm start to evolve from 650 mV. After adding glucose, two peaks at 280 and 362 nm are found until the potential reaches 750 mV. Those two peaks are identified as the characteristic peaks of CuO [60], which are produced due to the OER-coupled reaction. The difference in CuO formation potential observed after glucose introduction suggests that glucose electrooxidation is dominant below 750 mV. From the spectrum of Ni(II), a broad peak at 535 nm evolves from 450 mV, and another at 359 nm from 850 mV. The former is assigned to $Ni(OH)_2$ [59], and the latter indicates NiOOH. The disappearance of $Ni(OH)_2$ after injecting glucose suggests the dominating Ni(II)-glucose coordination, while an only negligible indication of NiOOH at 359 nm persists at 950 mV, where OER starts.

3.5 Glucose electrooxidation mechanism

(Figure 7)

Based on the above analysis, the glucose electrooxidation mechanism *via* transition metal ion is proposed in **Figure 7**. Upon the glucose addition to the electrolyte containing metal ion species M(II), the M(II)-glucose complex is formed *via* the coordination between *d* orbitals of metal and the electron donating hydroxy group (OH) of glucose (structure **1** shown in **Figure 7a**). Such a complex is engaged as the reactant in the double layer region with a finite diffusion manner. After electron transfer from the complex to the electrode, an intermediate complex evolves (structure **2** in **Figure 7a**) featuring a high valent metal species coordinated by glucose.

For Cu and Ni (**Figures 7a** and **7b**), the structure of M(III)-glucose is not stable and would go through structural rearrangement, producing a more energetically stable M(II)-gluconolactone complex (concentration distribution is shown as line **3** in **Figure 7a**). Eventually, the gluconate ion is produced with the regeneration of M(II). The components previously used in the equivalent electrical circuit (**Figure 4d**) can be related to different steps illustrated in **Figure 7b**. The mass transfer of M(II)-glucose from bulk to electrode surface is described by the Warburg resistance (Z_w) featuring a finite-length diffusion pattern, which is followed by electrooxidation described by R_{ct}. As suggested by EIS results, the reaction rate is kinetically controlled by the charge transfer rate from M(II)-glucose to the GCE (for detailed values, see **Table 1**).

In the case of Co, two intermediates are expected at a high applied potential (>600 mV), namely Co(III)-glucose and Co(IV)-glucose (**Figures 7c** and **7d**). The successive electrooxidation of Co(II)-glucose to Co(III)-glucose and Co(IV)-glucose is suggested by the Tafel plots, and R_{ct} describes its overall charge transfer process. The dissociation of Co(III)-gluconolactone complex regenerates Co(III) species within the double layer region to form Co(III)-glucose intermediate in a new cycle, and its transfer process is represented by the mass transfer resistance Z_w.

4. Conclusions

To conclude, the electrooxidation of glucose catalyzed by homogenously dispersed transition metal ions (Co, Cu, and Ni) in the alkaline electrolyte is studied. In the presence of glucose, the oxidation potential of M(II) to its higher valent species decreases, due to the formation of the metal-glucose complex where the OH- groups are replaced by glucose molecules. Under the same conditions, the activity trend of Co(II) > Cu(II) > Ni(II) is suggested by the cyclic voltammetric and chronoamperometric studies. As per glucose sensing properties, Co(II) shows a sensitivity of 1,342 mA M^{-1} cm^{-2}, while 579 and 38.9 mA M^{-1} cm^{-2} are achieved by using μM level Cu(II) and Ni(II), respectively. The EIS investigations reveal that no heterogonous coating layer is formed on the electrode surface during the reaction, and a homogenous electrooxidation mechanism with rate-determining charge transfer process is suggested for Co, Cu, and Ni. Evidences from *in situ* UV-Vis spectroelectrochemical studies confirm that the extensively formed M(II)-glucose complex is engaged for the electrooxidation other than M(II) hydroxide, and the OER route is blocked by coordinated glucose molecules. Co(II)-catalyzed reaction shows a potential-dependent electrooxidation *via* the formation of Co(III)-glucose and Co(IV)-glucose complex, while both Cu(II) and Ni(II) feature an intermediate of M(III)-glucose. The Co(II)-glucose electrooxidation presents the smallest charge transfer resistance and the highest charge transfer coefficient compared with Cu(II)-glucose and Ni(II)-glucose, an explanation of its high activity.

Acknowledgments

This work was supported by the Innovation and Technology Commission of Hong Kong and the Hong Kong Polytechnic University.

Supporting Information

The Pourbaix diagrams of Co, Cu, and Ni, the study of the reference electrode effect, Cu(I) species electrooxidation, *i*-t test, EIS results, and the in situ SPECE experiment setup and blank

test are available in supporting information.

Conflict of Interest

The authors declare no conflict of interest.

ORCID

Dr. Weiran Zheng 0000-0002-9915-6982

Dr. Lawrence Yoon Suk Lee 0000-0002-6119-4780

Author contribution

Dr. W. Zheng designed and conducted the electrochemical experiments (CV, EIS, and *in situ* SPECE) and data analysis, Y. Li performed the *i*-t test. Dr. L. Y. S. Lee supervised the progress of this project and drafted the manuscript with Dr. W. Zheng.

References

[1] D.W. Hwang, S. Lee, M. Seo, T.D. Chung, Recent Advances in Electrochemical Non-Enzymatic Glucose Sensors - a Review, Anal. Chim. Acta, 1033 (2018) 1-34. https://doi.org/10.1016/j.aca.2018.05.051

[2] K. Eid, Y.H. Ahmad, S.Y. AlQaradawi, N.K. Allam, Rational Design of Porous Binary Pt-Based Nanodendrites as Efficient Catalysts for Direct Glucose Fuel Cells over a Wide pH Range, Catal. Sci. Technol., 7 (2017) 2819-2827. https://doi.org/10.1039/C7CY00860K

[3] M. Frei, C. Kohler, L. Dietel, J. Martin, F. Wiedenmann, R. Zengerle, S. Kerzenmacher, Pulsed Electrodeposition of Highly Porous Pt Alloys for Use in Methanol, Formic Acid, and Glucose Fuel Cells, ChemElectroChem, 5 (2018) 1013-1023. https://doi.org/10.1002/celc.201800035

[4] X.G. Peng, G.P. Wan, L.H. Wu, M. Zeng, S.W. Lin, G.Z. Wang, Peroxidase-Like Activity of Au@TiO_2 Yolk-Shell Nanostructure and Its Application for Colorimetric Detection of H_2O_2 and Glucose, Sens. Actuators, B, 257 (2018) 166-177. https://doi.org/10.1016/j.snb.2017.10.146

[5] B.D. Hong, K.L. Hunag, H.R. Chen, C.L. Lee, Effect of Defective Graphene Flake for Catalysts of Supported Pd Nanocubes toward Glucose Oxidation Reaction in Alkaline Medium, J. Electrochem. Soc., 163 (2016) H731-H737. https://doi.org/10.1149/2.0141609jes

[6] Y. Wang, J. Chen, C.P. Zhou, L. Zhou, Y.Y. Kong, H.Y. Long, S.A. Zhong, A Novel Self-Cleaning, Non-Enzymatic Glucose Sensor Working under a Very Low Applied Potential Based on a Pt Nanoparticle-Decorated TiO_2 Nanotube Array Electrode, Electrochim. Acta, 115 (2014) 269-276. https://doi.org/10.1016/j.electacta.2013.09.173

[7] N. Hui, J.S. Wang, Electrodeposited Honeycomb-Like Cobalt Nanostructures on Graphene Oxide Doped Polypyrrole Nanocomposite for High Performance Enzymeless Glucose Sensing, J. Electroanal. Chem., 798 (2017) 9-16. https://doi.org/10.1016/j.jelechem.2017.05.021

[8] W. Zheng, L. Hu, L.Y.S. Lee, K.-Y. Wong, Copper Nanoparticles/Polyaniline/Graphene Composite as a Highly Sensitive Electrochemical Glucose Sensor, J. Electroanal. Chem., 781 (2016) 155-160. https://doi.org/10.1016/j.jelechem.2016.08.004

[9] Z.Y. Yang, Y.Q. Miao, T.R. Wang, X.C. Liang, M.S. Xiao, W.W. Li, Y. Yang, The Self-Adsorption of Ni Ultrathin Layer on Glassy Carbon Surface and Their Electrocatalysis toward Glucose, J. Electrochem. Soc., 161 (2014) H375-H378. https://doi.org/10.1149/2.049406jes

[10] D.F. Jiang, Z.Y. Chu, J.M. Peng, J.Y. Luo, Y.Y. Mao, P.Q. Yang, W.Q. Jin, One-Step Synthesis of Three-Dimensional $Co(OH)_2$/RGO Nano-Flowers as Enzyme-Mimic Sensors for Glucose Detection, Electrochim.

Acta, 270 (2018) 147-155. https://doi.org/10.1016/j.electacta.2018.03.066
[11] R. Madhu, V. Veeramani, S.-M. Chen, A. Manikandan, A.-Y. Lo, Y.-L. Chueh, Honeycomb-Like Porous Carbon–Cobalt Oxide Nanocomposite for High-Performance Enzymeless Glucose Sensor and Supercapacitor Applications, ACS Appl. Mater. Interfaces, 7 (2015) 15812-15820. https://doi.org/10.1021/acsami.5b04132
[12] K.L. Jiao, Z.P. Kang, B. Wang, S.Q. Jiao, Y. Jiang, Z.Q. Hu, Applying Co_3O_4@Nanoporous Carbon to Nonenzymatic Glucose Biofuel Cell and Biosensor, Electroanalysis, 30 (2018) 525-532. https://doi.org/10.1002/elan.201700719
[13] M.J. Song, S.K. Lee, J.H. Kim, D.S. Lim, Non-Enzymatic Glucose Sensor Based on Cu Electrode Modified with CuO Nanoflowers, J. Electrochem. Soc., 160 (2013) B43-B46. https://doi.org/10.1149/2.037304jes
[14] R. Li, X.J. Liu, H. Wang, Y. Wu, K.C. Chan, Z.P. Lu, Sandwich Nanoporous Framework Decorated with Vertical CuO Nanowire Arrays for Electrochemical Glucose Sensing, Electrochim. Acta, 299 (2019) 470-478. https://doi.org/10.1016/j.electacta.2019.01.033
[15] X. Wang, C.Y. Ge, K. Chen, Y.X. Zhang, An Ultrasensitive Non-Enzymatic Glucose Sensors Based on Controlled Petal-Like CuO Nanostructure, Electrochim. Acta, 259 (2018) 225-232. https://doi.org/10.1016/j.electacta.2017.10.182
[16] Y.Q. Ji, J. Liu, X.N. Liu, M.M.F. Yuen, X.Z. Fu, Y. Yang, R. Sun, C.P. Wong, 3D Porous Cu@Cu_2O Films Supported Pd Nanoparticles for Glucose Electrocatalytic Oxidation, Electrochim. Acta, 248 (2017) 299-306. https://doi.org/10.1016/j.electacta.2017.07.100
[17] M.H. Raza, K. Movlaee, Y.L. Wu, S.M. El-Refaei, M. Karg, S.G. Leonardi, G. Neri, N. Pinna, Tuning the NiO Thin Film Morphology on Carbon Nanotubes by Atomic Layer Deposition for Enzyme-Free Glucose Sensing, ChemElectroChem, 6 (2019) 383-392. https://doi.org/10.1002/celc.201801420
[18] M.L. Chelaghmia, M. Nacef, A.M. Affoune, M. Pontie, T. Derabla, Facile Synthesis of $Ni(OH)_2$ Modified Disposable Pencil Graphite Electrode and Its Application for Highly Sensitive Non-Enzymatic Glucose Sensor, Electroanalysis, 30 (2018) 1117-1124. https://doi.org/10.1002/elan.201800002
[19] Y.H. Yang, K. Yan, J.D. Zhang, Dual Non-Enzymatic Glucose Sensing on $Ni(OH)_2/TiO_2$ Photoanode under Visible Light Illumination, Electrochim. Acta, 228 (2017) 28-35. https://doi.org/10.1016/j.electacta.2017.01.050
[20] J.T.C. Barragan, S. Kogikoski, Jr., E. da Silva, L.T. Kubota, Insight into the Electro-Oxidation Mechanism of Glucose and Other Carbohydrates by CuO-Based Electrodes, Anal. Chem., 90 (2018) 3357-3365. https://doi.org/10.1021/acs.analchem.7b04963
[21] B. Xue, K.Z. Li, L. Feng, J.H. Lu, L.L. Zhang, Graphene Wrapped Porous $Co_3O_4/NiCo_2O_4$ Double-Shelled Nanocages with Enhanced Electrocatalytic Performance for Glucose Sensor, Electrochim. Acta, 239 (2017) 36-44. https://doi.org/10.1016/j.electacta.2017.04.005
[22] H. Heidari, E. Habibi, Amperometric Enzyme-Free Glucose Sensor Based on the Use of a Reduced Graphene Oxide Paste Electrode Modified with Electrodeposited Cobalt Oxide Nanoparticles, Microchim. Acta, 183 (2016) 2259-2266. https://doi.org/10.1007/s00604-016-1862-z
[23] S. Darvishi, M. Souissi, F. Karimzadeh, M. Kharaziha, R. Sahara, S. Ahadian, Ni Nanoparticle-Decorated Reduced Graphene Oxide for Non-Enzymatic Glucose Sensing: An Experimental and Modeling Study, Electrochim. Acta, 240 (2017) 388-398. https://doi.org/10.1016/j.electacta.2017.04.086
[24] R.M. Yuan, H.J. Li, X.M. Yin, H.Q. Wang, J.H. Lu, L.L. Zhang, Coral-Like Cu-Co-Mixed Oxide for Stable Electro-Properties of Glucose Determination, Electrochim. Acta, 273 (2018) 502-510. https://doi.org/10.1016/j.electacta.2018.04.003
[25] S. Bilal, W. Ullah, A.U.A. Shah, Polyaniline@CuNi Nanocomposite: A Highly Selective, Stable and Efficient Electrode Material for Binder Free Non-Enzymatic Glucose Sensor, Electrochim. Acta, 284 (2018) 382-391. https://doi.org/10.1016/j.electacta.2018.07.165
[26] A. Esmaeeli, A. Ghaffarinejad, A. Zahedi, O. Vahidi, Copper Oxide-Polyaniline Nanofiber Modified Fluorine Doped Tin Oxide (FTO) Electrode as Non-Enzymatic Glucose Sensor, Sens. Actuators, B, 266 (2018) 294-301. https://doi.org/10.1016/j.snb.2018.03.132
[27] M.J. Wang, X.F. Song, B. Song, J.L. Liu, C.G. Hu, D.P. Wei, C.P. Wong, Precisely Quantified Catalyst Based on in situ Growth of Cu_2O Nanoparticles on a Graphene 3D Network for Highly Sensitive Glucose Sensor, Sens. Actuators, B, 250 (2017) 333-341. https://doi.org/10.1016/j.snb.2017.04.125
[28] H. Naeim, F. Kheiri, M. Sirousazar, A. Afghan, Ionic Liquid/Reduced Graphene Oxide/Nickel-Palladium Nanoparticle Hybrid Synthesized for Non-Enzymatic Electrochemical Glucose Sensing, Electrochim. Acta, 282 (2018) 137-146. https://doi.org/10.1016/j.electacta.2018.05.204
[29] A.L. Sun, J.B. Zheng, Q.L. Sheng, A Highly Sensitive Non-Enzymatic Glucose Sensor Based on Nickel and

Multi-Walled Carbon Nanotubes Nanohybrid Films Fabricated by One-Step Co-Electrodeposition in Ionic Liquids, Electrochim. Acta, 65 (2012) 64-69. https://doi.org/10.1016/j.electacta.2012.01.007
[30] W. Zheng, Y. Li, M. Liu, C.-S. Tsang, L.Y.S. Lee, K.-Y. Wong, Cu^{2+}-Doped Carbon Nitride/MWCNT as an Electrochemical Glucose Sensor, Electroanalysis, 30 (2018) 1446-1454. https://doi.org/10.1002/elan.201800076
[31] Y.X. Li, X.H. Niu, J. Tang, M.B. Lan, H.L. Zhao, A Comparative Study of Nonenzymatic Electrochemical Glucose Sensors Based on Pt-Pd Nanotube and Nanowire Arrays, Electrochim. Acta, 130 (2014) 1-8. https://doi.org/10.1016/j.electacta.2014.02.123
[32] A.M. Ghonim, B.E. El-Anadouli, M.M. Saleh, Electrocatalytic Glucose Oxidation on Electrochemically Oxidized Glassy Carbon Modified with Nickel Oxide Nanoparticles, Electrochim. Acta, 114 (2013) 713-719. https://doi.org/10.1016/j.electacta.2013.10.115
[33] Y. Li, M.W. Xie, X.P. Zhang, Q. Liu, D.M. Lin, C.G. Xu, F.Y. Xie, X.P. Sun, Co-MOF Nanosheet Array: A High-Performance Electrochemical Sensor for Non-Enzymatic Glucose Detection, Sens. Actuators, B, 278 (2019) 126-132. https://doi.org/10.1016/j.snb.2018.09.076
[34] X. Zhang, J.S. Luo, P.Y. Tang, J.R. Morante, J. Arbiol, C.L. Xu, Q.F. Li, J. Fransaer, Ultrasensitive Binder-Free Glucose Sensors Based on the Pyrolysis of in situ Grown Cu MOF, Sens. Actuators, B, 254 (2018) 272-281. https://doi.org/10.1016/j.snb.2017.07.024
[35] G.C. Zang, W.T. Hao, X.Y. Li, S.H. Huang, J. Gan, Z. Luo, Y.C. Zhang, Copper Nanowires-MOFs-Graphene Oxide Hybrid Nanocomposite Targeting Glucose Electro-Oxidation in Neutral Medium, Electrochim. Acta, 277 (2018) 176-184. https://doi.org/10.1016/j.electacta.2018.05.016
[36] W.W. Li, S. Lv, Y. Wang, L. Zhang, X.Q. Cui, Nanoporous Gold Induced Vertically Standing 2D Nico Bimetal-Organic Framework Nanosheets for Non-Enzymatic Glucose Biosensing, Sens. Actuators, B, 281 (2019) 652-658. https://doi.org/10.1016/j.snb.2018.10.150
[37] W. Zheng, Y. Li, C.-S. Tsang, L. Hu, M. Liu, B. Huang, L.Y.S. Lee, K.-Y. Wong, Cu^{II}-Mediated Ultra-Efficient Electrooxidation of Glucose, ChemElectroChem, 4 (2017) 2788-2792. https://doi.org/10.1002/celc.201700712
[38] W. Zheng, Y. Li, L. Hu, L.Y.S. Lee, Use of Carbon Supports with Copper Ion as a Highly Sensitive Non-Enzymatic Glucose Sensor, Sens. Actuators, B, 282 (2019) 187-196. https://doi.org/10.1016/j.snb.2018.10.164
[39] L. Wang, X.P. Lu, Y.J. Ye, L.L. Sun, Y.H. Song, Nickel-Cobalt Nanostructures Coated Reduced Graphene Oxide Nanocomposite Electrode for Nonenzymatic Glucose Biosensing, Electrochim. Acta, 114 (2013) 484-493. https://doi.org/10.1016/j.electacta.2013.10.125
[40] H.G. Meier, J.R. Vilche, A.J. Arvía, The Electrochemical Behaviour of Cobalt in Alkaline Solutions Part Ii. The Potentiodynamic Response of $Co(OH)_2$ Electrodes, J. Electroanal. Chem. Interfacial Electrochem., 138 (1982) 367-379. https://doi.org/10.1016/0022-0728(82)85088-2
[41] J.M. Marioli, T. Kuwana, Electrochemical Characterization of Carbohydrate Oxidation at Copper Electrodes, Electrochim. Acta, 37 (1992) 1187-1197. https://doi.org/10.1016/0013-4686(92)85055-P
[42] O. Diaz-Morales, D. Ferrus-Suspedra, M.T.M. Koper, The Importance of Nickel Oxyhydroxide Deprotonation on Its Activity Towards Electrochemical Water Oxidation, Chem. Sci., 7 (2016) 2639-2645. https://doi.org/10.1039/c5sc04486c
[43] F. Song, X. Hu, Ultrathin Cobalt-Manganese Layered Double Hydroxide Is an Efficient Oxygen Evolution Catalyst, J. Am. Chem. Soc., 136 (2014) 16481-16484. https://doi.org/10.1021/ja5096733
[44] Y. Li, L. Hu, W. Zheng, X. Peng, M. Liu, P.K. Chu, L.Y.S. Lee, Ni/Co-Based Nanosheet Arrays for Efficient Oxygen Evolution Reaction, Nano Energy, 52 (2018) 360-368. https://doi.org/10.1016/j.nanoen.2018.08.010
[45] L.-A. Stern, X. Hu, Enhanced Oxygen Evolution Activity by NiO_x and $Ni(OH)_2$ Nanoparticles, Faraday Discuss., 176 (2014) 363-379. https://doi.org/10.1039/C4FD00120F
[46] Y. Deng, A.D. Handoko, Y. Du, S. Xi, B.S. Yeo, In Situ Raman Spectroscopy of Copper and Copper Oxide Surfaces During Electrochemical Oxygen Evolution Reaction: Identification of Cu^{III} Oxides as Catalytically Active Species, ACS Catal., 6 (2016) 2473-2481. https://doi.org/10.1021/acscatal.6b00205
[47] Y. Su, H. Guo, Z.S. Wang, Y.M. Long, W.F. Li, Y.F. Tu, Au@Cu_2O Core-Shell Structure for High Sensitive Non-Enzymatic Glucose Sensor, Sens. Actuators, B, 255 (2018) 2510-2519. https://doi.org/10.1016/j.snb.2017.09.056
[48] Y.L. Du, Y.F. He, Z.X. Zheng, X. Shen, Y.X. Zhou, T.X. Wang, Z.P. Zhu, C.M. Wang, A Renewable Platform for High-Performance Glucose Sensor Based on $Co(OH)_2$ Nanoparticles/Three-Dimensional Graphene Frameworks, J. Electrochem. Soc., 166 (2019) B42-B48. https://doi.org/10.1149/2.0481902jes
[49] P. Chakraborty, S. Dhara, K. Debnath, S.P. Mondal, Glucose and Hydrogen Peroxide Dual-Mode

Electrochemical Sensing Using Hydrothermally Grown CuO Nanorods, J. Electroanal. Chem., 833 (2019) 213-220. https://doi.org/10.1016/j.jelechem.2018.11.060

[50] Y.M. Sun, Y.X. Li, N. Wang, Q.Q. Xu, L. Xu, M. Lin, Copper-Based Metal-Organic Framework for Non-Enzymatic Electrochemical Detection of Glucose, Electroanalysis, 30 (2018) 474-478. https://doi.org/10.1002/elan.201700629

[51] C. Heyser, R. Schrebler, P. Grez, New Route for the Synthesis of Nickel(II) Oxide Nanostructures and Its Application as Non-Enzymatic Glucose Sensor, J. Electroanal. Chem., 832 (2019) 189-195. https://doi.org/10.1016/j.jelechem.2018.10.054

[52] X. Wu, F.L. Li, C.J. Zhao, X.Z. Qian, One-Step Construction of Hierarchical $Ni(OH)_2$/RGO/Cu_2O on Cu Foil for Ultra-Sensitive Non-Enzymatic Glucose and Hydrogen Peroxide Detection, Sens. Actuators, B, 274 (2018) 163-171. https://doi.org/10.1016/j.snb.2018.07.141

[53] N. Pal, S. Banerjee, A. Bhaumik, A Facile Route for the Syntheses of $Ni(OH)_2$ and NiO Nanostructures as Potential Candidates for Non-Enzymatic Glucose Sensor, J. Colloid Interface Sci., 516 (2018) 121-127. https://doi.org/10.1016/j.jcis.2018.01.027

[54] E. Barsoukov, J.R. Macdonald, Impedance Spectroscopy: Theory, Experiment, and Applications, 2nd ed., Wiley-Interscience, Hoboken, N.J., 2005.

[55] T.Q. Nguyen, C. Breitkopf, Determination of Diffusion Coefficients Using Impedance Spectroscopy Data, J. Electrochem. Soc., 165 (2018) E826-E831. https://doi.org/10.1149/2.1151814jes

[56] A.J. Bard, L.R. Faulkner, Electrochemical Methods: Fundamentals and Applications, 2nd ed., Wiley, New York, 2001.

[57] L.M. Alrehaily, J.M. Joseph, M.C. Biesinger, D.A. Guzonas, J.C. Wren, Gamma-Radiolysis-Assisted Cobalt Oxide Nanoparticle Formation, Phys. Chem. Chem. Phys., 15 (2013) 1014-1024. https://doi.org/10.1039/c2cp43094k

[58] F. Lyu, Y. Bai, Q. Wang, L. Wang, X. Zhang, Y. Yin, Phase-Controllable Synthesis of Cobalt Hydroxide for Electrocatalytic Oxygen Evolution, Dalton Trans., 46 (2017) 10545-10548. https://doi.org/10.1039/c7dt01110e

[59] M. Vidotti, C. van Greco, E.A. Ponzio, S.I. Córdoba de Torresi, Sonochemically Synthesized $Ni(OH)_2$ and $Co(OH)_2$ Nanoparticles and Their Application in Electrochromic Electrodes, Electrochem. Commun., 8 (2006) 554-560. https://doi.org/10.1016/j.elecom.2006.01.024

[60] X.Y. Chen, H. Cui, P. Liu, G.W. Yang, Shape-Induced Ultraviolet Absorption of CuO Shuttlelike Nanoparticles, Appl. Phys. Lett., 90 (2007). https://doi.org/10.1063/1.2736285

List of Figures

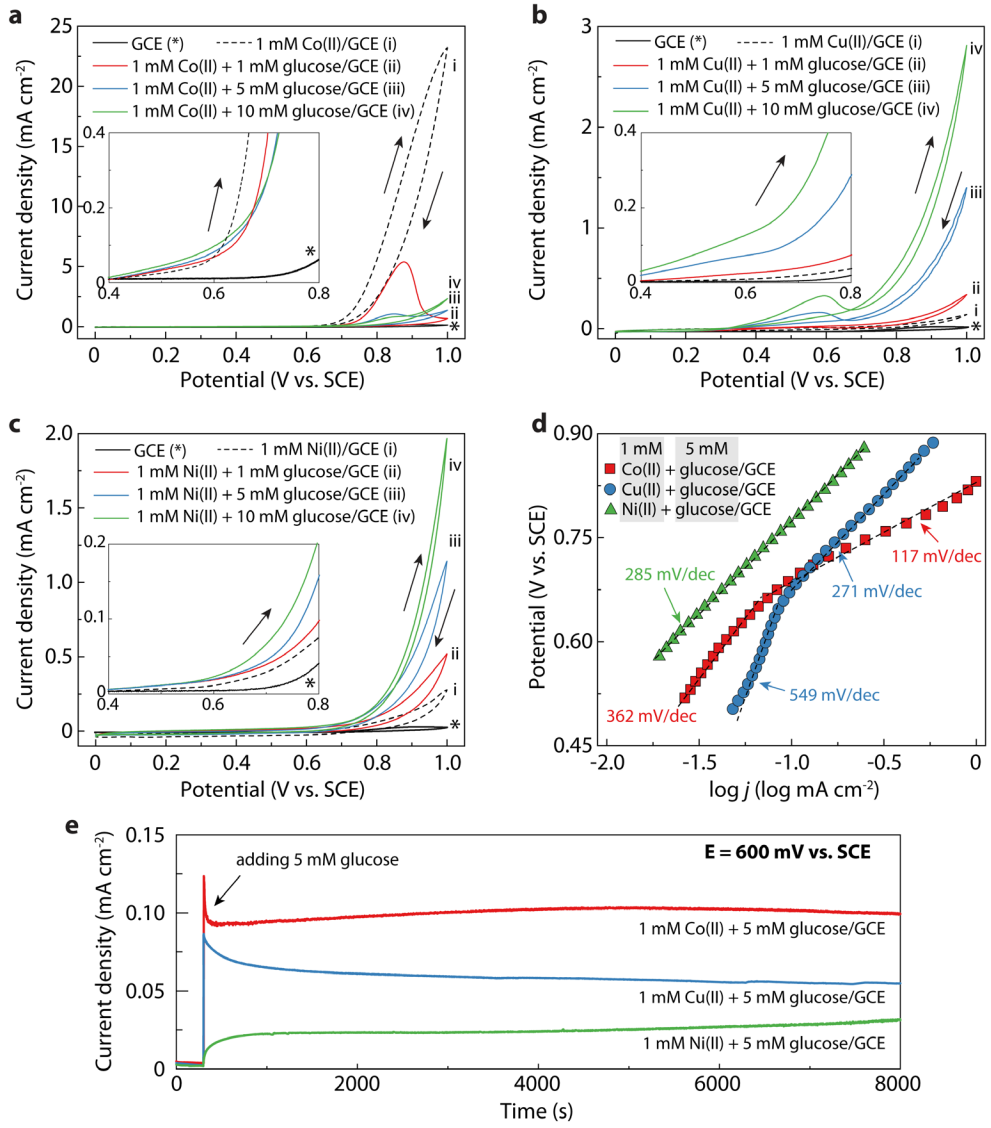

Figure 1. (a-c) CV plots of GCE in 0.1 M NaOH solution containing 1 mM M(II) (dotted line) and 1 mM M(II) + glucose (1 mM, 5 mM, and 10 mM) (solid line): (a) Co; (b) Cu; (c) Ni. Only the first cycles are shown for clarity. Insets show the enlarged forward scan between 0.40 and 0.80 V. The CV plot of GCE in 0.1 M NaOH is shown in black solid line for reference; (d) Tafel plots of glucose electrooxidation catalyzed by 1 mM Co(II), Cu(II), and Ni(II) in the presence of 5 mM glucose. (e) Stability test of glucose electrooxidation using 1 mM Co(II), Cu(II), and Ni(II) with 5 mM glucose. Applied potential is 600 mV in all tests.

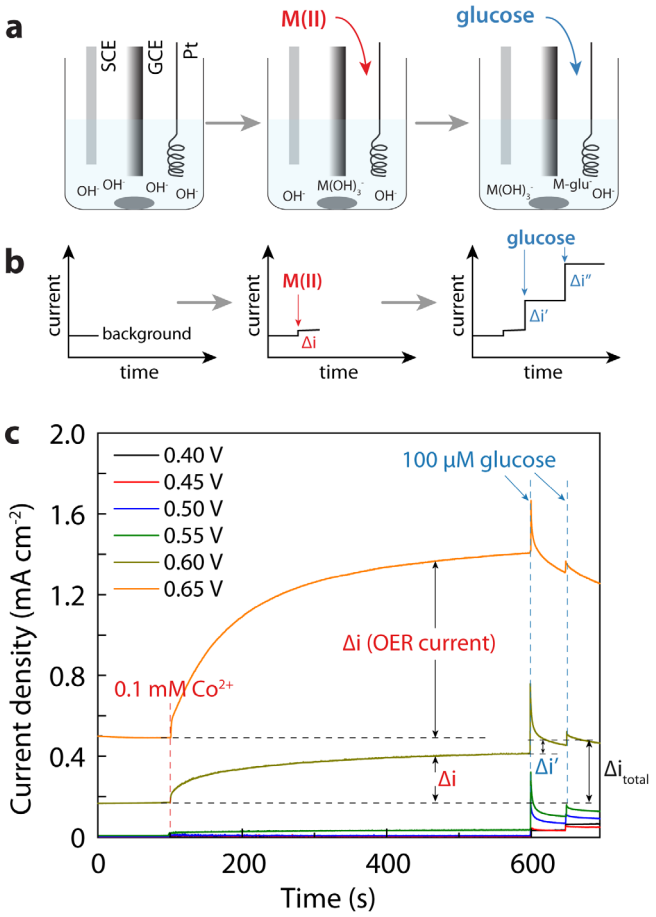

Figure 2. (a) Illustration of procedures of using M(II) for glucose electrooxidation; (b) Illustration of the corresponding amperometric responses upon the introduction of M(II) and glucose; (c) Amperometric responses of bare GCE in 0.1 M NaOH at different applied potentials with 0.1 mM Co(II) and 0.1 mM glucose added stepwise.

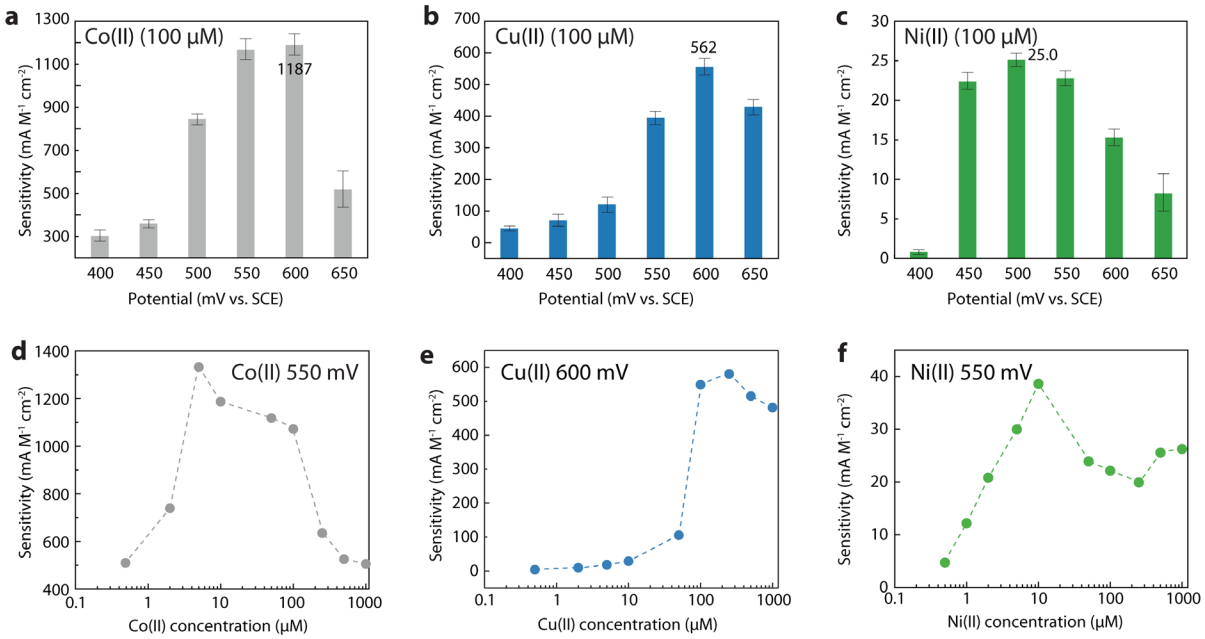

Figure 3. (a-c) The sensitivity of glucose detection at variou applied potentials using GCE in 0.1 M NaOH solution containing 0.1 mM M(II): (a) Co; (b) Cu; (c) Ni. Sensitivity values are calculated based on three amperometric tests; (d-f) The sensitivity of glucose detection at a selected applied potential using GCE in 0.1 M NaOH solution containing different concentrations of M(II) (0.5 μM ~ 1.0 mM): (d) Co at 550 mV; (e) Cu at 600 mV; (f) Ni at 550 mV.

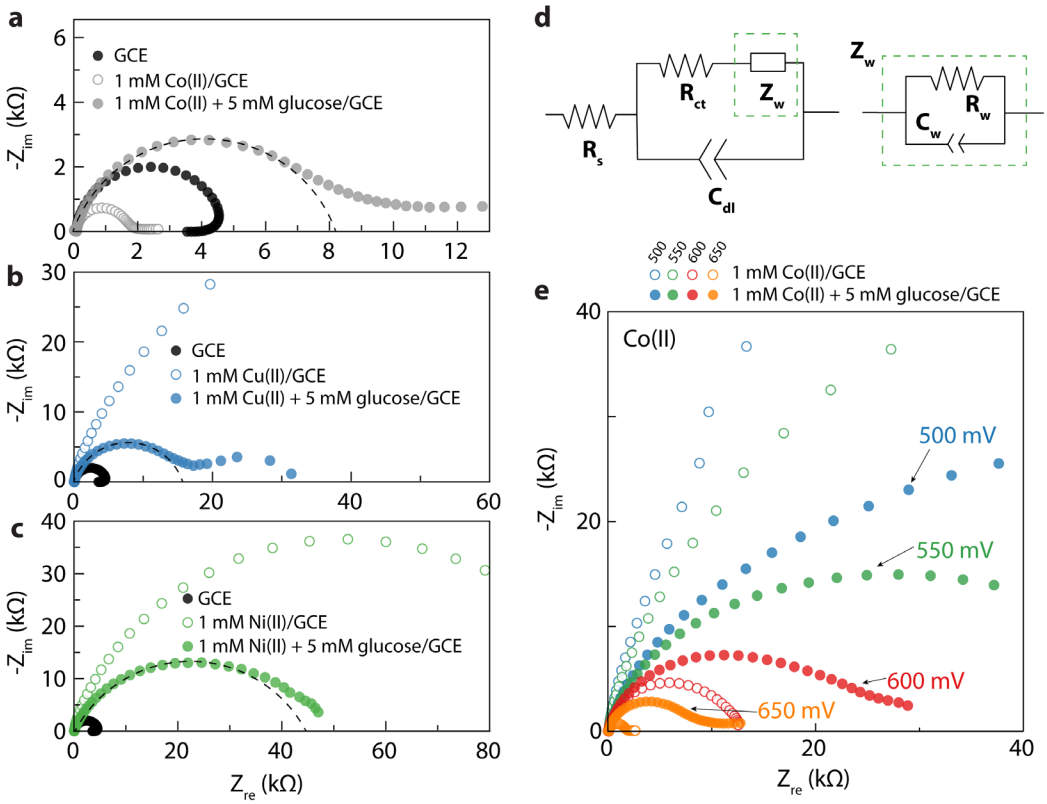

Figure 4. Nyquist plots of GCE at 650 mV in 0.1 mM NaOH solution containing 1 mM M(II) (hollow circle) and 1 mM M(II) + 5 mM glucose (solid circle): (a) Co; (b) Cu; (c) Ni. The plots of GCE in 0.1 M NaOH is shown as reference (black solid circle). Dotted lines show the fitted half cycles; (d) Equivalent electrical circuit employed for impedance spectroscopic analysis. (e) Nyquist plots of GCE at various applied potentials (500, 550, 600, and 650 mV) in 0.1 mM NaOH solution containing 1 mM Co(II) (hollow circle) and 1 mM Co(II) + 5 mM glucose (solid circle).

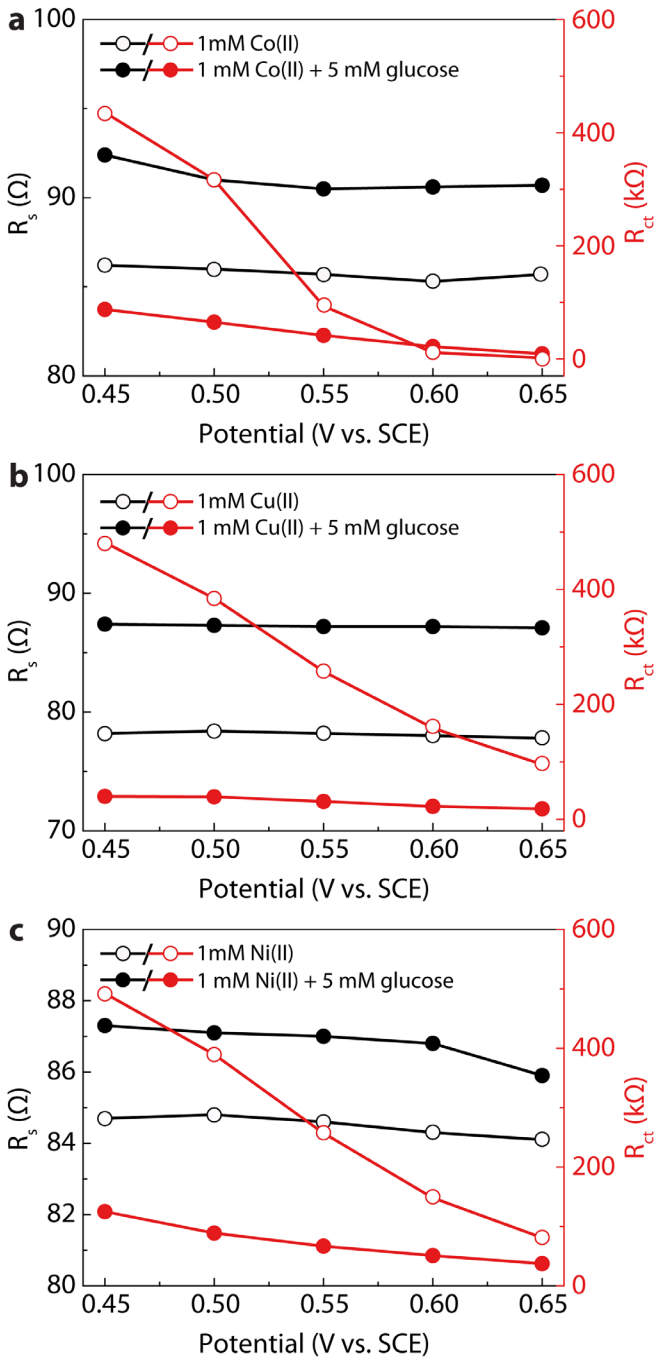

Figure 5. Fitted R_s (black circles) and R_{ct} (red circles) values of the corresponding Nyquist plots under different applied potentials obtained using GCE in 0.1 M NaOH solution containing 1 mM M(II) (hollow circles) and 1 mM M(II) + 5 mM glucose (solid circles): (a) Co; (b) Cu; (c) Ni.

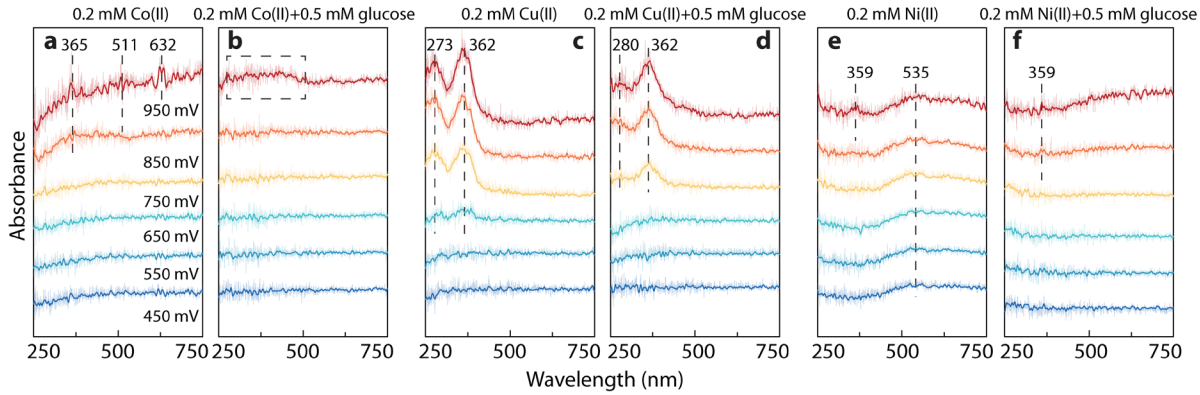

Figure 6. Background-subtracted *in situ* electrochemical UV-Vis spectra at various applied potentials in 0.1 M NaOH containing: (a) 0.2 mM Co(II); (b) 0.2 mM Co(II) + 0.5 mM glucose; (c) 0.2 mM Cu(II); (d) 0.2 mM Cu(II) + 0.5 mM glucose; (e) 0.2 mM Ni(II); (f) 0.2 mM Ni(II) + 0.5 mM glucose. The spectra at 0 V are used as the background.

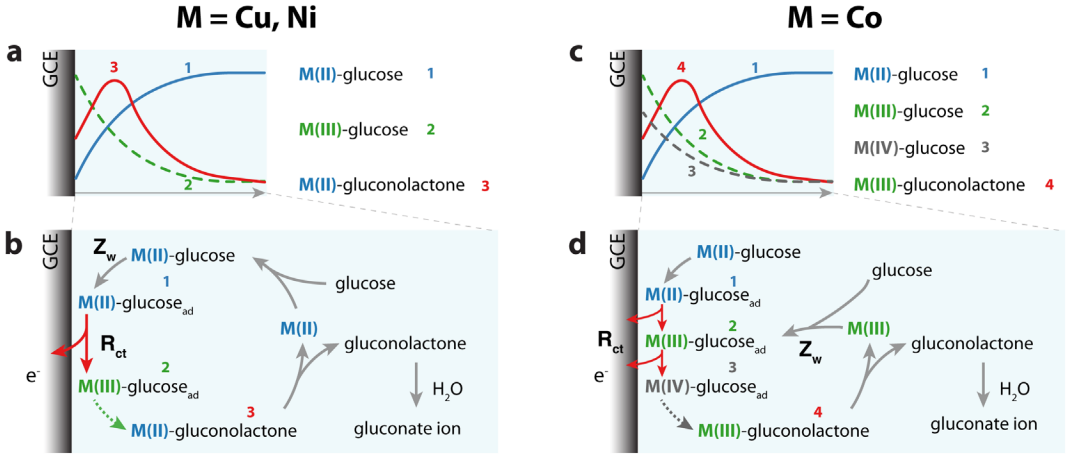

Figure 7. Proposed double layer structure during metal ion-mediated glucose electrooxidation: (a) Cu, Ni; (c) Co; Proposed mechanism of metal ion-mediated glucose electrooxidation: (b) Cu, Ni; (d) Co.

Table 1. Kinetic aspects of glucose electrooxidation catalyzed by transition metal ions.

	Co	**Cu**	**Ni**
Tafel slope[1] (mV dec^{-1})	362 (0.52 ~ 0.65 V) 117 (0.65 ~ 0.82 V)	549 (0.50 ~ 0.64 V) 271 (0.64 ~ 0.90 V)	285 (0.60 ~ 0.90 V)
Charge transfer coefficient[2] α	0.157 (0.52 ~ 0.65 V) 0.503 (0.65 ~ 0.82 V)	0.107 (0.50 ~ 0.64 V) 0.219 (0.64~0.90 V)	0.209 (0.60 ~ 0.90 V)
Best sensitivity[3] (mA M^{-1} cm^{-2})	1342 (5 μM, 0.55 V)	579 (200 μM, 0.60 V)	38.9 (10 μM, 0.55 V)
Charge transfer resistance[4] (kΩ)	8.98	18.4	37.4

[1] Tafel slope is obtained from CV with a scan rate of 5 mV s^{-1}, M(II) concentration of 1 mM, and a glucose concentration of 5 mM.

[2] Charge transfer coefficients are calculated from the total current *i*, following $\alpha = \frac{RT}{F} \cdot \frac{1}{dE/dlni} = \frac{2.3RT}{F} \cdot \frac{1}{dE/dlogi}$.

[3] Best sensitivity values are obtained at selected M(II) concentration and voltage bias.

[4] Charge transfer resistances are calculated based on EIS results at 0.65 V where 1 mM M(II) and 5 mM glucose are used.

Graphical abstract